

# Investigation of Torque Ripple in Voltage Source Inverter driven Induction Motor Drive operated with Space Vector based Harmonic Elimination Pulse Width Modulation Scheme

Rohan Sandeep Burye

*School of Electrical Sciences  
Indian Institute of Technology Goa,  
Ponda, India  
rohan19242205@iitgoa.ac.in*

Ravi Teja Arumalla

*Dept. of Electrical and Electronics Engineering  
Rajiv Gandhi University of  
Knowledge and Technology,  
Ongole, India  
ravitejaeee.89@gmail.com*

Sheron Figarado

*School of Electrical Sciences  
Indian Institute of Technology Goa,  
Ponda, India  
sheron@iitgoa.ac.in*

**Abstract**—The lower order harmonic elimination using space vector pulse width modulation (SVPWM) technique is possible by introducing the dwell time division coefficient ‘ $k$ ’ in space vector. In this paper, torque ripple analysis is carried out for space vector based harmonic elimination (SVHE) scheme and the obtained results are compared with the existing schemes such as conventional and advance bus clamping SVPWM schemes. Further, the obtained results are validated through simulation results. The SVHE scheme gives the lower torque ripple than the conventional and advance bus clamping schemes at higher modulation indices.

**Index Terms**—Space vector pulse width modulation, total harmonic distortion, torque ripple, harmonic elimination, voltage source inverter.

## I. INTRODUCTION

The torque ripple is a significant performance metric in variable-speed induction motor (IM) drive systems[1]. According to [2], the torque ripple in an IM drive is caused by the harmonic content in an inverter’s output waveform. In [3], a time-domain method of analysis based on the concept of stator flux ripple is proposed to analyse the harmonic distortion caused by space vector based PWM approaches. In addition, [4] proposes an analytical method for predicting torque ripple of an IM drive running at low pulse number. The selection of pulse width modulation (PWM) techniques to trigger the inverter switches determines the quality of the inverter’s output waveform [5]. Over these years various PWM schemes are devised for low, medium and high frequency applications. An extensive review on various PWM techniques for motor drive application is presented in [6].

One of the most popular PWM technique is selective harmonic elimination (SHE). The SHE permits elimination of certain lower order harmonics which are dominant component of the torque ripple. It is especially useful in high power, low frequency application [7]. The SHE requires solving the transcendental equations obtained through fourier analysis. Hence, the real time implementation of SHE is challenging

task in dynamic conditions. Using Groebner bases and symmetric polynomial theory, an algebraic method is proposed to solve transcendental equations associated with SHE in [8]. Unlike traditional numerical methods, this method gives all the possible solutions and had no requirements on choosing initial value.

The most widely used PWM method for real time implementation is sinusoidal pulse width modulation (SPWM). In this method a sinusoidal reference waveform is compared with a high frequency carrier waveform to generate PWM. The advantage of this method is its simplicity and ease of implementation with microcontroller. By adding appropriate common mode voltage it is possible to generate a conventional and bus clamping SVPWM sequences. A phase shifted SPWM to reduce common mode voltage in multi-phase two level inverter is proposed in [9]. A FPGA-based implementation of SPWM strategy for high frequency inverter is presented in [10]. A zero voltage switching based SPWM modulation scheme is proposed for grid connected Inverter in [11]. The analytical and graphical method to generate carrier-based PWM is extensively reviewed in [12].

The space vector pulse width modulation(SV-PWM) is an immensely popular method for a three phase 2-level VSI. Both carrier based and space vector based PWM can implement conventional and clamping sequences. But SPWM fails to implement advance bus clamping (ABC-PWM) sequences. Therefore, space vector based PWM is more general than triangle comparison method of generating PWM. Moreover, SVPWM has higher DC bus utilization than SPWM. The SVPWM techniques depend on the sequence in which the space vectors are applied. An overview of different SVPWM techniques can be found in [13]. The most popular space vector based PWM techniques are conventional space vector PWM(CSV-PWM), bus clamping PWM(BC-PWM) and advance bus clamping PWM(ABC-PWM).

In the CSV-PWM, the dwell time associated with the zero

vector is divided equally among zero vectors  $V_0$  and  $V_7$ . The CSV-PWM has 3 switchings per subcycle. The CSV-PWM offers the best total harmonic distortion (THD) performance. The bus clamping sequences utilize two active vector and a zero vector in a sector resulting into 2 switchings per subcycle. The bus clamping sequences clamp one of the phase to the DC bus for a  $60^\circ$  duration in a subcycle which leads to lower switching losses and reduction in current ripple of an inverter [14]. With respect to the clamping duration, bus clamping is further classified as continual and split clamping. An analysis based on the torque ripple and harmonic distortion of continual clamp and split-clamp PWM for IM drive is shown in [15]. It is shown that optimal positioning of the clamping interval in split-clamp PWM yield better results in terms of lower torque ripple and THD in line current than all other bus clamping sequences. In Advance bus clamping sequences an active vector is applied twice in a subcycle and it has shown to reduce THD compared to the conventional and bus clamping switching sequence at higher modulation indices [16].

The ABC-PWM can offer improved torque ripple profile at higher modulation index. Thus, the space vector based hybrid PWM technique is proposed in [1], wherein combination of CSV-PWM and ABC-PWM sequences is used for different regions of a sector in the space vector diagram. In [17], a PWM technique is proposed that is a combination of optimal continuous modulation and discontinuous modulation and has been demonstrated to reduce torque ripple by 30%. In [18], four space-vector-based hybrid PWM approaches are suggested, which reduce line current distortion and switching loss in IM drives when compared to CSV-PWM.

The unequal division of the dwell times associated with the space vectors in SVPWM technique can lead to sequences having less torque ripple for certain modulation indices. Moreover, this dwell time division also makes elimination of particular lower order harmonics possible which result in lower torque ripple. The Space Vector sequences generated using this concept of dwell time arrangement are called space vector harmonic elimination sequences (SVHE). The SVHE offers advantage of both SHE and SVPWM techniques. The concept of eliminating harmonics using space vector first appeared in [19]. A model predictive switching pattern control to eliminate the lower order harmonics based on space vector approach was proposed in [20] for current source converter.

The objective of this paper is to perform the torque ripple analysis on a SVHE sequence which is formulated by using the concept of dwell time rearrangement to selectively eliminate a particular lower order harmonic [21]. The performance of this sequence with regards to torque ripple are compared with the CSV-PWM and ABC-PWM techniques. All of the switching sequences under consideration are having 18 switchings/phase/fundamental cycle which ensures near equal switching loss and makes the comparison fair. The analytically obtained and simulated torque ripple waveforms are presented.

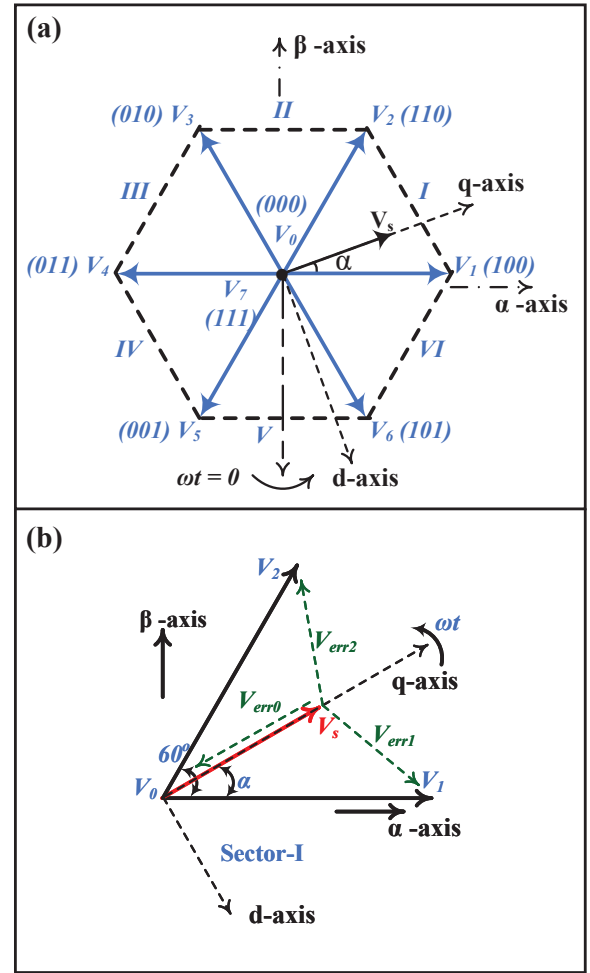


Fig. 1: (a)SV Diagram (b)Error voltage vectors in sector-1

## II. ANALYSIS OF TORQUE RIPPLE

The Fig. 1(a) shows Space Vector diagram for a three phase 2 level VSI. It consist of six active vectors ( $V_1$ - $V_7$ ) and zero vectors ( $V_0$  and  $V_7$ ) forming a Hexagon. The Sector-1 of SV diagram along with the error voltages are shown in Fig. 1(b). Any reference vector ( $V_{ref}$ ) within the sector-1 is realized by switching active vectors  $V_1$ ,  $V_2$  and zero vectors  $V_0$ ,  $V_7$  for duration  $T_1$ ,  $T_2$  and  $T_0$  respectively. This is called volt-sec balance. The dwell timings are calculated as

$$T_1 = \frac{V_{ref} \sin(60^\circ - \alpha)}{V_{dc} \sin(60^\circ)} T_s \quad (1a)$$

$$T_2 = \frac{V_{ref} \sin(\alpha)}{V_{dc} \sin(60^\circ)} T_s \quad (1b)$$

$$T_0 = T_s - T_1 - T_2 \quad (1c)$$

$$T_s = \frac{1}{300nm} \quad (1d)$$

$$V_{ref} = 0.866mV_{dc} \quad (1e)$$

TABLE I: SVPWM Sequences under study

Sequence	SPS	Sequence	Dwell Time Arrangement
CSV	3 (10°, 30°, 50°)	0127-7210-0127	$T_0.T_1.T_2.T_7-T_7.T_2.T_1.T_0-T_0.T_1.T_2.T_7$
ABC-I	2 (15°, 45°)	0121-1210	$T_0.0.5T_1.T_2.0.5T_1-0.5T_1.T_2.T_1.0.5T_0$
ABC-II	2 (15°, 45°)	7212-2127	$T_7.0.5T_2.T_1.0.5T_2-T_2.T_1.0.5T_2.T_7$
SVHE	2 (15°, 45°)	0121-7212	$T_0.kT_1.T_2.(1-k)T_1-T_7.(1-k)T_2.T_1.kT_2$

where,

$m$  = modulation index  
 $n$  = number of sample in a sector  
 $T_s$  = sample duration  
 $V_{dc}$  = DC link voltage of the Inverter

The different SVPWM sequences under consideration are tabulated in Table I.

In CSV, the zero vector dwell time is divided equally among  $T_0$  and  $T_7$  which gives best THD results. The ABC-I and ABC-II are double switching sequences in which active vector is applied twice in a subcycle. The SVHE sequence proposed in [21] uses a dwell time re-arrangement with a factor  $k$  to selectively eliminate either a 5<sup>th</sup> or 7<sup>th</sup> harmonic. The value of  $k$  is found by solving the non-linear algebraic equations obtained from the fourier analysis of the pole voltage [21]. The sample per sector (SPS) and the dwell time arrangement for each of the sequences is also shown in Table I.

The torque ripple waveforms are obtained using the notion of stator flux ripple [3]. In this method, the error voltage vector is resolved along q-axis and the d-axis of a synchronously rotating reference frame, with the q-axis aligned along  $V_{ref}$  (see Fig. 1). The q-axis component of error voltage vector for SVHE sequence is derived and given by eqs. (2) and (3). Similarly, it can be obtained for other sequences listed in Table I.

$$\tilde{v}_{q,0121} = \begin{cases} K_1 & 0 < t < T_0 \\ K_2 + K_1 & T_0 < t < T_0 + kT_1 \\ K_3 + K_1 & T_0 + kT_1 < t < T_0 + kT_1 + T_2 \\ K_2 + K_1 & T_0 + kT_1 + T_2 < t < T_s \end{cases} \quad (2)$$

$$\tilde{v}_{q,7212} = \begin{cases} K_1 & T_s < t < T_s + T_7 \\ K_3 + K_1 & T_s + T_7 < t < T_s + T_7 + (1-k)T_2 \\ K_2 + K_1 & T_s + T_7 + (1-k)T_2 < t < 2T_s - kT_2 \\ K_3 + K_1 & 2T_s - kT_2 < t < 2T_s \end{cases} \quad (3)$$

where,

$$\begin{aligned} K_1 &= -V_{ref} \\ K_2 &= V_{dc} \cos(\alpha) \\ K_3 &= V_{dc} \cos(60^\circ - \alpha) \end{aligned}$$

The time integral of  $\tilde{v}_q$  gives the q-axis stator flux ripple ( $\tilde{\psi}_q$ ), which is an indicator of q-axis current ripple  $\tilde{i}_q$ . The analytical expression for q-axis stator flux ripple for the SVHE is evaluated and obtained in eqs. (4) and (5).

$$\tilde{\psi}_{q,0121} = \begin{cases} K_1 t & 0 < t < T_0 \\ K_4 t - K_2 T_0 & T_0 < t < T_0 + kT_1 \\ \begin{cases} K_2(kT_1) + (K_5)t \\ -K_3(T_0 + kT_1) \end{cases} & \begin{cases} T_0 + kT_1 < t \\ < T_s - (1-k)T_1 \end{cases} \\ \begin{cases} (K_4)(t - T_2) \\ -K_2 T_0 + (K_5)T_2 \end{cases} & T_s - (1-k)T_1 < t < T_s \end{cases} \quad (4)$$

$$\tilde{\psi}_{q,7212} = \begin{cases} K_1(t - T_s) & T_s < t < T_s + T_7 \\ (K_5)(t - T_s) - K_3 T_7 & \begin{cases} T_s + T_7 < t < T_s \\ + T_7 + (1-k)T_2 \end{cases} \\ \begin{cases} (K_6)(T_7 + (1-k)T_2) \\ -K_3 T_7 + (K_4)(t - T_s) \end{cases} & \begin{cases} T_s + T_7 + (1-k)T_2 \\ < t < 2T_s - kT_2 \end{cases} \\ \begin{cases} (K_5)(t - T_s - T_1) \\ -K_3 T_7 + (K_4)T_1 \end{cases} & 2T_s - kT_2 < t < 2T_s \end{cases} \quad (5)$$

where,

$$\begin{aligned} K_4 &= K_2 + K_1 \\ K_5 &= K_3 + K_1 \\ K_6 &= K_3 - K_2 \end{aligned}$$

Similarly, the stator flux ripple for other sequences listed in Table I is obtained. Torque ripple is produced when  $i_q$  interacts with fundamental flux along the d-axis, according to [1]. As a result, the ripple in an Induction motor's produced torque ( $\tilde{\tau}_d$ ) is given by

$$\tilde{\tau}_d = \frac{2}{3} \cdot \frac{P}{2} \cdot \frac{V_{ref}}{2\pi f_1} \cdot \frac{1}{L_O} \cdot \left[ \frac{1}{\sigma_s + \sigma_r} - 1 \right] \tilde{\psi}_q \quad (6)$$

Here,  $\sigma$  is the ratio of total leakage inductance to the magnetizing inductance of the motor [17].

The parameters of the Induction motor used for the simulation are given in Table II.

By inspection of torque ripple waveform for SVHE and CSV sequence, it is inferred that the torque ripple for SVHE depends solely on the  $T_0$  whereas in case of CSV it depends on the  $T_0$  and  $T_2$ . This is true for the uniform sampling locations

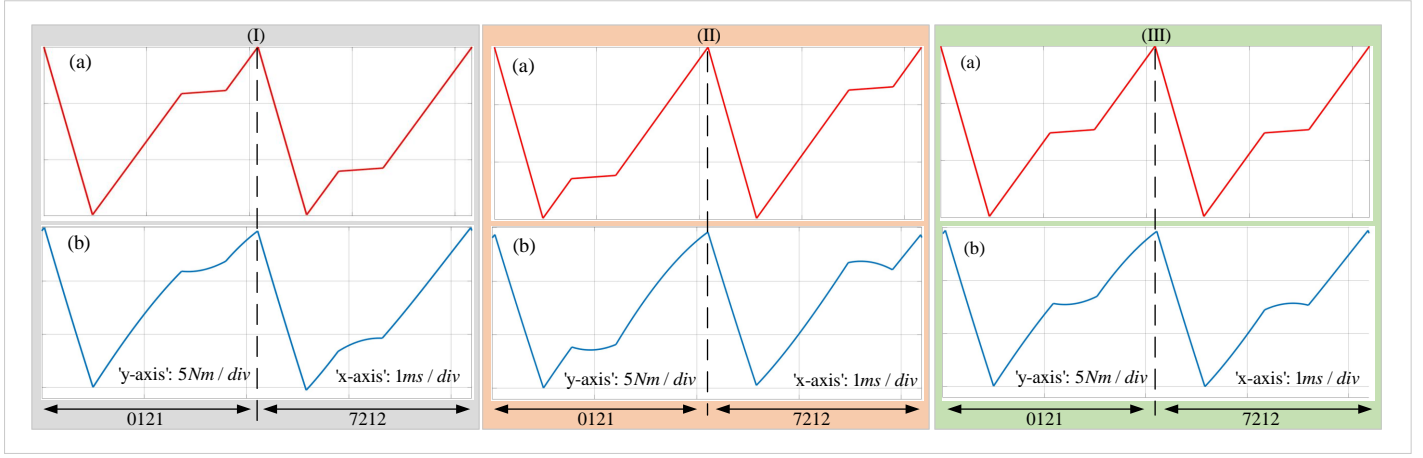


Fig. 2: Torque ripple waveforms of SVHE sequence 0121-7212: (a)analytical & (b)simulation for (I) 5<sup>th</sup> elimination, (II) 7<sup>th</sup> elimination & (III) No harmonic elimination ( $k = 0.5$ ) case at 0.8 modulation index

TABLE II: Parameters of Induction Motor

Parameter	Value
Rated Power, $P_{rated}$	7.5 kW
Stator Resistance, $R_s$	1.1667 $\Omega$
Rotor Resistance, $R_r$	3.2105 $\Omega$
Magnetizing Inductance, $L_O$	0.3025 H
Stator leakage coefficient, $\sigma_s$	0.0392
Rotor leakage coefficient, $\sigma_r$	0.0392

as specified in Table I. Thus, an expression for peak to peak q-axis stator flux ripple is derived for SVHE and given by (7).

$$\begin{aligned}\Delta\tilde{\psi}_{q,SVHE} &= V_{ref} \cdot T_{0,SVHE} \\ &= V_{ref}T_{s1}(1 - m(\sin(\alpha_1) + \sin(60^\circ - \alpha_1)))\end{aligned}\quad (7)$$

where,

$$\begin{aligned}\text{Sample-1 duration of SVHE}(T_{s1}) &= \frac{1}{600m} \\ \text{Sample-1 location of SVHE}(\alpha_1) &= 15^\circ\end{aligned}$$

Similarly, expression for the peak to peak q-axis stator flux ripple is derived for CSV and given by (8).

$$\begin{aligned}\Delta\tilde{\psi}_{q,CSV} &= V_{ref} \cdot T_{0,CSV} + 2(V_{ref} - V_{dc})T_{2,CSV} \\ &= T_{s2} \times [V_{ref}(1 - m(\sin(\alpha_2) + \sin(60^\circ - \alpha_2))) \\ &\quad + (V_{ref} - V_{dc}\cos(60^\circ - \alpha_2))2m\sin(\alpha_2)]\end{aligned}\quad (8)$$

where,

$$\begin{aligned}\text{Sample-1 duration of CSV}(T_{s2}) &= \frac{1}{900m} \\ \text{Sample-1 location of CSV}(\alpha_2) &= 10^\circ\end{aligned}$$

The magnitude of peak-to-peak torque developed( $\Delta\tilde{\tau}_d$ ) corresponding to these stator flux ripple is obtained from (6).

The expression for range of modulation indices for which  $\Delta\tilde{\psi}_{q,SVHE} < \Delta\tilde{\psi}_{q,CSV}$  and is obtained in (9).

$$m > \frac{0.5 + \frac{2\sin(\alpha_2)\cos(60^\circ - \alpha_2)}{\cos(30^\circ)}}{1.5(\sin(\alpha_1) + \sin(60^\circ - \alpha_1)) + \sin(\alpha_2) - \sin(60^\circ - \alpha_2)}\quad (9)$$

The torque ripple in IM drive is independent of the d-axis ripple and is related to the q-axis ripple. However,  $F_d$  and  $F_q$ , where  $F_d$  and  $F_q$  are the RMS of the d-axis ripple and q-axis flux ripple waveforms, respectively, have an equivalent impact on the THD of the motor current waveform. Thus, a decrease in q-axis ripple denotes a decrease in both THD and in torque ripple, but a decrease in d-axis ripple solely denotes a decrease in THD.

The THD in the motor current is a useful indicator of current ripples [3]. The current THD is defined as (10), where  $I_1$  and  $I_n$  are the RMS of the no load current's fundamental and  $n^{th}$  harmonic component, respectively.

$$I_{THD} = \frac{1}{I_1} \sum_{n=2}^{\infty} I_n\quad (10)$$

Unlike q-axis ripple, the peak-to-peak magnitude of the d-axis ripple ( $\Delta\tilde{\psi}_d$ ) is independent of the modulation index for SVHE and CSV sequences. The  $\Delta\tilde{\psi}_d$  for SVHE is found to be lower than the CSV sequence. Although the  $\Delta\tilde{\psi}_d$  is independent of the dwell time arrangement, the  $F_d$  depends on the dwell time division coefficient ' $k$ '.

### III. RESULTS AND DISCUSSION

The analytical expression for  $\tilde{\psi}_q$  is evaluated for each of the SV-PWM sequences listed in Table I and corresponding torque ripple waveform  $\tilde{\tau}_d$  is obtained using Symbolic Math in MATLAB script. The analytically obtained peak-to-peak magnitude of torque ripple is compiled and the result is presented in Table III.

The torque ripple waveforms are also obtained from the IM model in MATLAB Simulink for these sequences and

TABLE III: Analytical results of torque ripple magnitude for Sequence-CSV:0127-7210-0127,ABC-I:0121-1210,ABC-II:7212-2127, and SVHE:0121-7212

Modulation Index	Peak-to-peak ripple magnitude( $Nm$ )					
	CSV	ABC-I	ABC-II	SVHE		
	$H_{NE}$	$H_{NE}$	$H_{NE}$	$H_{NE}$	$H_5$	$H_7$
0.6	20.066	55.046	55.07	27.57	27.57	27.57
0.65	17.011	48.547	48.618	24.4	24.4	24.4
0.7	14.958	42.442	42.432	21.24	21.24	21.24
0.75	13.025	36.066	36.038	18.06	18.06	18.06
0.8	11.7	29.723	29.588	14.9	14.9	14.9
0.85	10.432	23.719	23.741	11.74	11.74	11.74
0.9	9.136	17.763	17.812	8.569	8.569	8.569
0.95	7.844	11.893	11.908	5.398	5.756	5.942

$H_{NE}$ : No harmonic elimination ( $k = 0.5$ )

$H_5$ : 5<sup>th</sup> harmonic elimination

$H_7$ : 7<sup>th</sup> harmonic elimination

TABLE IV: Simulation results of line current THD at no load for Sequence-CSV:0127-7210-0127 and SVHE:0121-7212

Modulation Index	Total harmonic distortion(%)			
	CSV	SVHE		
	$H_{NE}$	$H_{NE}$	$H_5$	$H_7$
0.6	71.84	87.83	84.57	97.71
0.65	68.32	79.67	75.96	90.96
0.7	65.12	71.85	67.58	84.34
0.75	62.32	64.45	59.48	78.23
0.8	59.95	57.82	52.01	72.64
0.85	58.06	52.22	45.36	67.68
0.9	56.9	47.62	39.67	63.31
0.95	56.43	44.84	35.78	60.03

$H_{NE}$ : No harmonic elimination ( $k = 0.5$ )

$H_5$ : 5<sup>th</sup> harmonic elimination

$H_7$ : 7<sup>th</sup> harmonic elimination

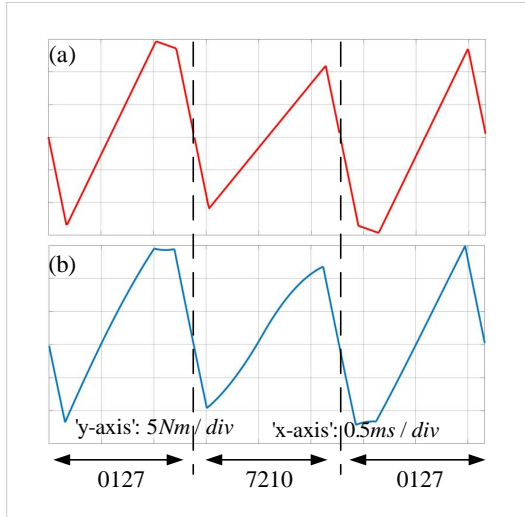


Fig. 3: Torque ripple waveforms of CSV sequence 0127-7210-0127: (a)analytical & (b)simulation at 0.8 modulation index

it is found in good agreement with the analytically obtained waveforms. The Fig. 2-5 shows the torque ripple waveforms obtained from the analytical method and MATLAB simulation

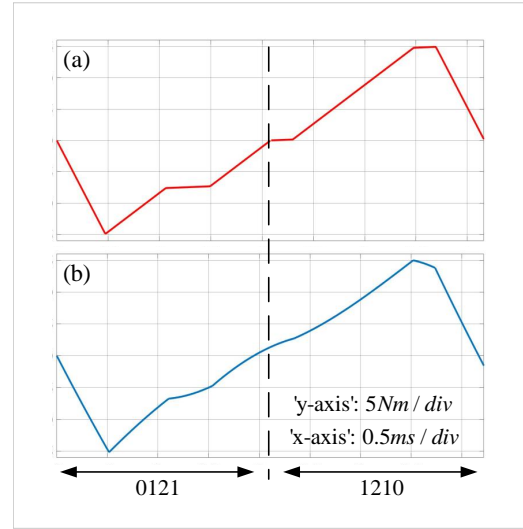


Fig. 4: Torque ripple waveforms of ABC-I sequence 0121-1210: (a)analytical & (b)simulation at 0.8 modulation Index

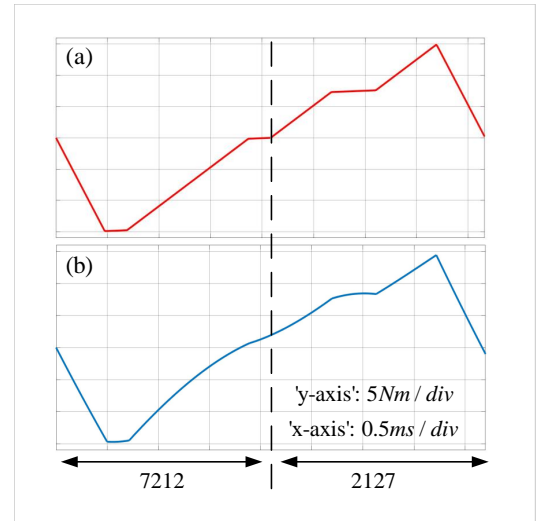


Fig. 5: Torque ripple waveforms of ABC-II sequence 7212-2127: (a)analytical & (b)simulation at 0.8 modulation index

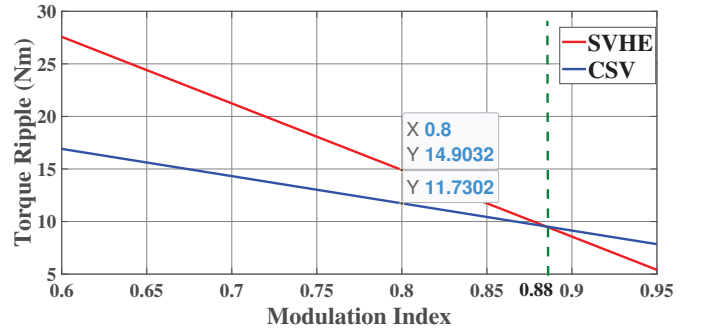


Fig. 6: Peak-to-peak torque ripple magnitude variation with modulation index for SVHE and CSV PWM sequences

for one sector duration for a modulation index of 0.8 and rated power of  $7.5kW$ . The sector duration is  $2T_s$  for 2 SPS(2 sample per sector) and  $3T_s$  for 3 SPS. This is valid only for uniform sampling case wherein duration between two consecutive samples is constant. Further the line current THD at no load condition is computed from the simulation, and the results are tabulated in Table IV. The following observations are made from tables III and IV:

- The SVHE sequence shows no change in the torque ripple magnitude for elimination and ‘no elimination’ case. This is due to relationship of magnitude with  $T_0$  duration alone as shown in (7) and the dwell time re-arrangement happens for the active vector duration.
- The SVHE gives better torque ripple performance compared to ABC-I and ABC-II for entire range of modulation Index.
- SVHE sequence gives better torque ripple than CSV at higher modulation index above 0.8847 as obtained by (9) and evident from Fig. 6.
- The torque ripple magnitude decreases with increase in modulation index for all the sequences. This is because as we increase the modulation index, the fundamental magnitude increases relative to harmonics.
- The  $I_{THD}$  for  $5^{th}$  harmonic elimination case in SVHE shows better results than CSV for modulation index above 0.7. This is due to the dependency of  $F_d$  on ‘ $k$ ’

#### IV. CONCLUSION

A torque ripple analysis using the notion of stator flux is presented. The torque ripple for a special Space Vector sequence called SVHE is evaluated and compared with the CSV-PWM and ABC-PWM. This special sequence can eliminate a particular harmonics using the dwell time rearrangement. The results from analytical and simulation are compared and validated. An analytical expression for the modulation index is derived above which the SVHE gives better results than CSV with respect to the torque ripple. The SVHE has shown better torque ripple performance compared to CSV-PWM at modulation index above 0.8847. The torque ripple are significantly reduced at higher modulation index as evident from the torque ripple waveforms. The SVHE with  $5^{th}$  harmonic elimination gives better  $I_{THD}$  than CSV for modulation index above 0.7.

#### REFERENCES

- [1] V. S. S. P. K. Hari and G. Narayanan, "Space-Vector-Based Hybrid PWM Technique to Reduce Peak-to-Peak Torque Ripple in Induction Motor Drives," in IEEE Transactions on Industry Applications, vol. 52, no. 2, pp. 1489-1499, March-April 2016.
- [2] A. Tripathi and G. Narayanan, "Evaluation and Minimization of Low-Order Harmonic Torque in Low-Switching-Frequency Inverter-Fed Induction Motor Drives," in IEEE Transactions on Industry Applications, vol. 52, no. 2, pp. 1477-1488, March-April 2016.
- [3] G. Narayanan and V. T. Ranganathan, "Analytical evaluation of harmonic distortion in PWM AC drives using the notion of stator flux ripple," in IEEE Transactions on Power Electronics, vol. 20, no. 2, pp. 466-474, March 2005.
- [4] A. Tripathi and G. Narayanan, "Analytical Evaluation and Reduction of Torque Harmonics in Induction Motor Drives Operated at Low Pulse Numbers," in IEEE Transactions on Industrial Electronics, vol. 66, no. 2, pp. 967-976, Feb. 2019.
- [5] R. T. Arumalla, S. Figarado and N. Harischandrapa, "Dodecagonal Voltage Space Vector Based PWM Techniques for Switching Loss Reduction in a Dual Inverter Fed Induction Motor Drive," in IEEE Journal of Emerging and Selected Topics in Industrial Electronics, vol. 1, no. 2, pp. 182-191, Oct. 2020.
- [6] Chen, Henglin, and Huan Zhao. "Review on pulse-width modulation strategies for common-mode voltage reduction in three-phase voltage-source inverters." IET Power Electronics 9.14 (2016).
- [7] M. S. A. Dahidah, G. Konstantinou and V. G. Agelidis, "A Review of Multilevel Selective Harmonic Elimination PWM: Formulations, Solving Algorithms, Implementation and Applications," in IEEE Transactions on Power Electronics, vol. 30, no. 8, pp. 4091-4106, Aug. 2015.
- [8] K. Yang, Q. Zhang, R. Yuan, W. Yu, J. Yuan and J. Wang, "Selective Harmonic Elimination With Groebner Bases and Symmetric Polynomials," in IEEE Transactions on Power Electronics, vol. 31, no. 4, pp. 2742-2752, April 2016.
- [9] Z. Liu, Z. Zheng, S. D. Sudhoff, C. Gu and Y. Li, "Reduction of Common-Mode Voltage in Multiphase Two-Level Inverters Using SPWM With Phase-Shifted Carriers," in IEEE Transactions on Power Electronics, vol. 31, no. 9, pp. 6631-6645, Sept. 2016.
- [10] M. Lakka, E. Koutroulis and A. Dollas, "Development of an FPGA-Based SPWM Generator for High Switching Frequency DC/AC Inverters," in IEEE Transactions on Power Electronics, vol. 29, no. 1, pp. 356-365, Jan. 2014.
- [11] Y. Chen et al., "A ZVS Grid-Connected Full-Bridge Inverter With a Novel ZVS SPWM Scheme," in IEEE Transactions on Power Electronics, vol. 31, no. 5, pp. 3626-3638, May 2016.
- [12] A. M. Hava, R. J. Kerkman and T. A. Lipo, "Simple analytical and graphical methods for carrier-based PWM-VSI drives," in IEEE Transactions on Power Electronics, vol. 14, no. 1, pp. 49-61, Jan. 1999.
- [13] Nandhini, E., and A. Sivaprakasam. "A Review of Various Control Strategies Based on Space Vector Pulse Width Modulation for the Voltage Source Inverter." IETE Journal of Research (2020): 1-15.
- [14] A. Kumar and D. Chatterjee, "A survey on space vector pulse width modulation technique for a two-level inverter," 2017 National Power Electronics Conference (NPEC), 2017.
- [15] Das, Soumitra, et al. "Analysis of generalized continual-clamp and split-clamp PWM schemes for induction motor drive." Sādhanā 44.2 (2019).
- [16] T. Bhavsar and G. Narayanan, "Harmonic Analysis of Advanced Bus-Clamping PWM Techniques," in IEEE Transactions on Power Electronics, vol. 24, no. 10, pp. 2347-2352, Oct. 2009.
- [17] K. Basu, J. S. S. Prasad and G. Narayanan, "Minimization of Torque Ripple in PWM AC Drives," in IEEE Transactions on Industrial Electronics, vol. 56, no. 2, pp. 553-558, Feb. 2009.
- [18] D. Zhao, V. S. S. P. K. Hari, G. Narayanan and R. Ayyanar, "Space-Vector-Based Hybrid Pulsewidth Modulation Techniques for Reduced Harmonic Distortion and Switching Loss," in IEEE Transactions on Power Electronics, vol. 25, no. 3, pp. 760-774, March 2010.
- [19] S. R. Bowes and S. Singh Grewal, "Novel space-vector-based harmonic elimination inverter control," in IEEE Transactions on Industry Applications, vol. 36, no. 2, pp. 549-557, March-April 2000.
- [20] H. Gao, B. Wu, D. Xu, R. P. Aguilera and P. Acuna, "Model Predictive Switching Pattern Control for Current-Source Converters With Space-Vector-Based Selective Harmonic Elimination," in IEEE Transactions on Power Electronics, vol. 32, no. 8, pp. 6558-6569, Aug. 2017.
- [21] R. T. Arumalla, S. Figarado, K. Panuganti and N. Harischandrapa, "Selective Lower Order Harmonic Elimination in DC-AC Converter Using Space Vector Approach," in IEEE Transactions on Circuits and Systems II: Express Briefs, vol. 68, no. 8, pp. 2890-2894, Aug. 2021.